NANOMATERIALS

Chemical vapor deposition synthesis of near-zigzag single-walled carbon nanotubes with stable tube-catalyst interface

Qiuchen Zhao,[1] Ziwei Xu,[2,3] Yue Hu,[1] Feng Ding,[2]* Jin Zhang[1]*

Chemical vapor deposition (CVD) growth is regarded as the most promising method for realizing structure-specific single-walled carbon nanotube (SWNT) growth. In the past 20 years, many efforts dedicated to chirality-selective SWNT growth using various strategies have been reported. However, normal CVD growth under constant conditions could not fully optimize the chirality because the randomly formed cap structure allows the nucleation of all types of SWNTs and the chirality of an SWNT is unlikely to be changed during the following elongation process. We report a new CVD process that allows temperature to be periodically changed to vary SWNT chirality multiple times during elongation to build up the energetically preferred SWNT-catalyst interface. With this strategy, SWNTs with small helix angles (less than 10°), which are predicted to have lower interfacial formation energy than others, are enriched up to ~72%. Kinetic analysis of the process suggests a multiple redistribution feature whereby a large chiral angle SWNT tends to reach the near-zigzag chirality step by step with a small chiral angle change at each step, and hence, we named this method "tandem plate CVD." This method opens a door to synthesizing chirality-selective SWNTs by rational catalyst design.

INTRODUCTION

Thermodynamics and kinetics are two key factors in controlling a chemical reaction, and certainly single-walled carbon nanotube (SWNT) growth is no exception (1). In recent years, intensive efforts have been dedicated to realize chirality-selective SWNT growth (2–10) through either thermodynamic control, such as building a more stable epitaxial interface between an SWNT and a catalyst or an SWNT seed (8, 9, 11, 12), or kinetic control, such as using the different growth rates of different SWNTs (13). Proceeding from the concept of thermodynamics, a catalyst particle with specific structure might provide a "template" for the nucleation of an SWNT (8, 9, 11, 12, 14, 15). For example, high–melting-point W-Co alloy can be used as a template to realize the chirality-controlled growth of SWNTs (8, 9). Similarly to epitaxial growth, "cloning growth" used SWNT seeds as templates to realize the growth of SWNTs with exactly the same structure (11, 12). Most of these efforts were based on the optimization of the SWNT-catalyst or the SWNT-seed interface for chirality-selective SWNT growth.

In principle, an SWNT with a more stable tube-catalyst interface certainly has a higher probability of being synthesized, and many previous theoretical calculations have confirmed that the tube-catalyst interfacial formation energy difference can be significant (16–21). Besides those high–melting point catalysts mentioned above, our systematic density functional calculations also showed that, for the commonly used efficient catalysts Fe, Co, and Ni, the near-zigzag SWNTs had much more stable SWNT-catalyst interfacial formation energy than others, about 0.1 eV/Å or 3 eV/tube for SWNTs with a diameter of ~1 nm.

Such a difference should, in principle, lead to a strong selectivity of >99.99% for the low chiral angle SWNTs calculated according to the thermodynamic distribution. On the other hand, most experiments with chirality selection using these efficient catalysts produced near armchair SWNTs (6, 22–26), such as (6,5), (7,5), (8,7), and (9,8) SWNTs. Such a contradiction between the experimental results and theoretical predictions leads to the question of whether these SWNTs were really enriched by thermodynamic preference. As we know, for SWNT growth, the first stage is the formation of a cap on the catalyst surface. It is known that any cap with less than six pentagons is immature. Certainly, during the initial nucleation stage, the cap-catalyst interface can be well optimized but such an optimization does not lead to any control of the SWNT chirality. When the sixth pentagon is incorporated into the rim of a cap, the cap becomes mature and the chirality of the SWNT is determined. Unfortunately, theoretical simulation proved that the formation energy of different cap structures is very similar and does not provide thermodynamic preference for SWNT chirality control (10). After a cap has become an infant SWNT, its chirality is difficult to change as proved experimentally and predicated theoretically (27, 28). This indicates that during common SWNT growth, there is no effective optimization of the SWNT chirality through the SWNT-catalyst interface formation.

The above argument strongly suggests that if the SWNT chirality could be further changed during the growth process, it might be possible to control the SWNT chirality by further optimizing the SWNT-catalyst interface, and realize a thermodynamically optimized SWNT structure. As predicted by theoretical calculations, the well optimized SWNT samples should be greatly enriched to near-zigzag ones. Therefore, we designed our experiment as shown in Fig. 1A. In contrast to the traditional CVD SWNT growth under constant experimental conditions, we induced a perturbation to the growth process. The structures of growing SWNTs could be changed probabilistically and their chiralities redistributed during growth. Certainly, we would

[1]Center for Nanochemistry, Beijing National Laboratory for Molecular Sciences, State Key Laboratory for Structural Chemistry of Unstable and Stable Species, College of Chemistry and Molecular Engineering, Peking University, Beijing 100871, China. [2]Institute of Textiles and Clothing, Hong Kong Polytechnic University, Hong Kong Special Administrative Region 999077, China. [3]School of Materials Science & Engineering, Jiangsu University, Zhenjiang 212013, China.
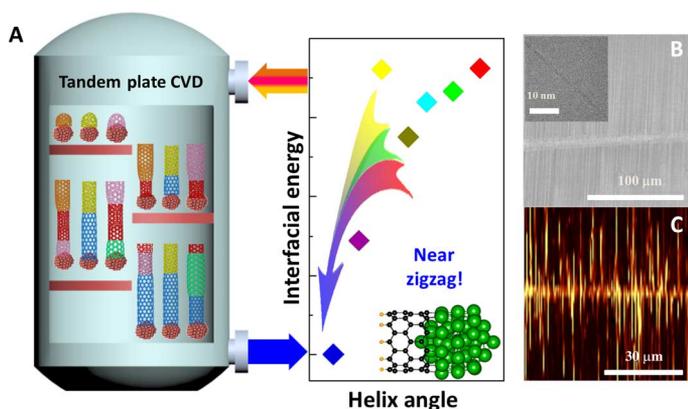*Corresponding author. Email: feng.ding@polyu.edu.hk (F.D.); jinzhang@pku.edu.cn (J.Z.)

Fig. 1. Schematic illustration and basic characterization of TPCVD method. (**A**) Schematic illustration of the TPCVD method. The temperature perturbation was realized by repeatedly changing the sample position in the furnace. This method used the interfacial formation energy between catalyst and SWNT, which was related to the helix angle of SWNTs in our system. (**B**) Scanning electron microscopy (SEM) and transmission electron microscopy (TEM) (inset) characterization of as-grown SWNT arrays from the TPCVD method. The tubes were transferred onto Si₃N₄ grids for TEM observation. (**C**) G-band Raman mapping of as-grown SWNT arrays after transfer onto a SiOₓ/Si substrate. The excitation laser frequency was 514 nm.

expect the new population distribution to gravitate more toward the thermodynamically preferred ones, which should be determined by the relative stabilities of the tube-catalyst interfaces. Thus, we expected the enrichment of zigzag SWNTs. Such a process is akin to what happens on a "plate" in the distillation column. Then, when multiple plates are cascaded together, that is, the perturbations are executed repeatedly, we could get a preponderant structure with lower interfacial formation energy. We call this new CVD method "tandem plate chemical vapor deposition" (TPCVD). In our TPCVD system, the key was to choose a repeatable and reliable perturbation method to change the SWNT chirality during growth which would not be so violent as to cause the sudden death of the catalysts. It has been reported that temperature variation could induce a structural change of SWNTs (*29*, *30*). Thus, we chose to vary the temperature during SWNT growth as an effective perturbation method. As the experimental temperature varied repeatedly, the chirality of an SWNT could be changed multiple times to the small helix angle side of the chiral map, exactly as we predicted theoretically.

RESULTS

In our experimental design, the temperature perturbation was operated by changing the relative sample position in a CVD furnace. As shown in fig. S1, in a CVD furnace, thermal diffusion led to a temperature decrease axially along the quartz tube from the center to both ends. By oscillating the furnace's position, the temperature around the substrate, where the SWNTs were growing, could be changed periodically. By carefully controlling the frequency and amplitude of the furnace's oscillation, a controllable temperature perturbation from 820° to 880°C was realized. For optimized SWNT growth, the temperature perturbation process was operated 90 times in 9 min. Figure 1 (B and C)

shows the characterization of as-grown SWNT horizontal arrays using the TPCVD method. SEM showed that the average length of the well-aligned grown SWNTs was more than 80 μm with very good orientation, and the density of SWNTs was about two to three tubes per micrometer. TEM characterization proved that our carbon nanotubes were single-walled, and the low D band in the Raman spectrum showed that the SWNTs were of high quality (see fig. S2). According to our previous work (*31*), SWNT growth followed the base growth mechanism under this CVD condition. This mechanism ensured that in an individual SWNT, the part near the catalyst stripe was grown later than that far from catalyst stripes. Thus, analyzing the tube structures near the catalyst stripes provided information on chirality enrichment after the TPCVD growth. The Raman spectrum with an excitation energy of 2.41 eV (514 nm) was used to characterize the chiralities of the SWNTs near the catalyst stripe, and the corresponding chirality distribution of the identified SWNTs is shown in Fig. 2B (*24*). The result showed that the SWNTs with an RBM shift of ~193 cm⁻¹ were drastically enriched. The chiralities of these tubes were revealed as either (16,0) or (15,2). Although these two SWNTs are difficult to distinguish with resonant RBM shifts for their similar electronic structures and diameters, the shapes of their G peaks are significantly different. It is well known that a semiconducting zigzag SWNT has a symmetrical Lorentz-shape G band (*9*). Our Raman spectra, however, provided asymmetric shapes of the G peaks, as shown in fig. S2. Thus, the chiral index of these greatly enriched SWNTs could be unambiguously assigned as (15,2). This is also in agreement with the theoretical analysis of the SWNT growth kinetics—the growth rates of zigzag tubes should be slower than those of other tubes by several orders of magnitude and thus must be rare (*13*, *32*). After associating each RBM peak to the chiral index, we calculated the helix angle of these tubes and finally got a distribution, which is shown in Fig. 2A. From this, we could see an overall trend with SWNTs having small chiral angles highly enriched. Among all the measured tubes shown in Fig. 2A, the population of SWNTs that have helix angles <10° was 72%. To further confirm this result, we took two more Raman mapping measurements with exciting lasers of 1.96 eV (633 nm) and 1.58 eV (785 nm). The results of the 633-nm laser are shown in figs. S2 and S3. Characterization with the 785-nm laser, however, provided very few resonant tubes and hence poor statistical significance, so those results were not shown. The measurements also demonstrated a similar enrichment of small helix angle SWNTs, which showed a population of ~75%. Although these excitation lasers cannot cover all the SWNT structures, we could still consider the smaller chiral angle SWNT enrichment as a universal behavior attributed to the chirality change during the TPCVD process, because the resonant phenomenon did not have chiral angle preferences. Furthermore, besides the (*n*,*m*) index, the structure of an SWNT can be indicated by other methods. By a simple polar coordinate transformation, (*n*,*m*) can be transferred into (*D*,θ) with the following equation (*33*)

$$D = a_{c\text{-}c} \times \frac{\sqrt{n^2 + nm + m^2}}{\pi} \tag{1}$$

$$\theta = \tan^{-1}[\sqrt{3}m/(2n + m)] \tag{2}$$

in which *D* refers to the diameter of an SWNT, θ refers to the helix angle, and $a_{c\text{-}c}$ refers to the length of the carbon-carbon bond. From
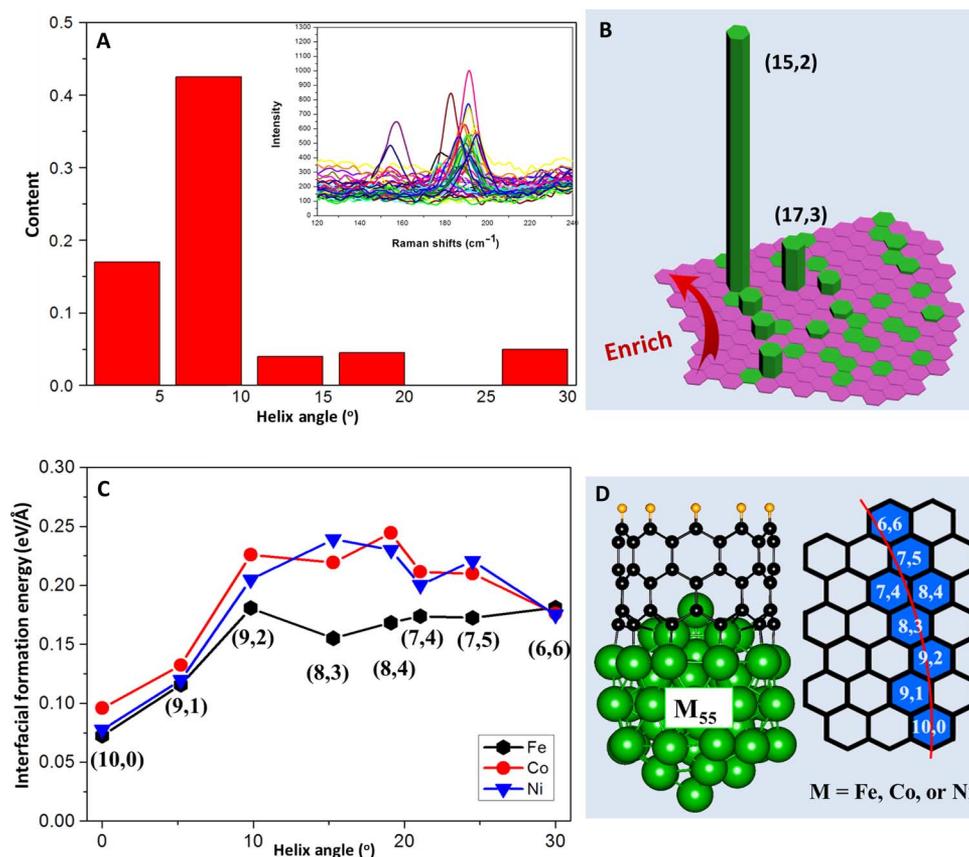
Fig. 2. Results and analysis of TPCVD methods. (**A**) Distribution of helix angle after a 90-cycle TPCVD process, which showed 72% content of SWNTs with small helix angle (<10°). Inset is the typical Raman spectra in a 50-μm line mapping. Radial breathing mode (RBM) peaks around 193 cm^{-1} are significantly enriched. (**B**) Chirality distribution of as-grown SWNT arrays analyzed by Raman spectroscopy. Hexagons in green refer to the chirality, which were resonant at 514 nm. More than 800 RBM signals were collected. (**C**) Density functional theory (DFT) calculation of the interfacial formation energy between SWNT and Fe, Co, and Ni catalysts. Small helix angle tubes (<10°) showed a lower interfacial energy among these three systems. (**D**) Models and diameter distributions of the simulation. Fe$_{55}$ was used as a catalyst, and the diameter of SWNTs was confined to about 0.8 nm to match the catalyst.

the equation, we can see that the structure of an SWNT could be controlled by the diameter and the helix angle. In our TPCVD system, we chose Fe as catalyst because of its high efficiency, which does not control the diameter directly. However, as the catalyst size accumulates spontaneously in a Gaussian distribution (*34*), we could also realize a significant chirality enrichment of (15,2) SWNTs experimentally. In a length of 600 μm near the catalyst stripe, we counted 117 resonant RBM signals of the (15,2) SWNTs. With SEM characterization, we found the total number of SWNTs to be 564 ± 17 in the same scanning area. Thus, the chirality selectivity of (15,2) tubes could be no less than 21%. This content was eight times higher than that from the normal CVD growth process, in which all the tube chiralities are nearly equally distributed. Although the yield was not very high, it clearly had potential as a means of achieving chirality control. It is worth mentioning that our measurement only counted the number of SWNTs near the catalyst stripe and the kinetics of SWNT growth, such as the growth rates and the lifetime of catalysts that did not contribute to the results (detailed illustrations are shown in fig. S4).

According to the previous design, the TPCVD method could enrich thermodynamically preferred SWNTs. For further information, DFT calculations were used to analyze the interfacial formation energy between SWNT and catalyst. Figure 2C shows the difference of interfacial formation energy between catalysts (Fe$_{55}$, Co$_{55}$, or Ni$_{55}$) and SWNTs. All the simulated tubes had similar diameter (~0.8 nm, which matches the size of M$_{55}$ catalyst) but different helix angles, as shown in Fig. 2D. For all three catalysts, SWNTs with helix angles <10° [such as (10,0) and (9,1) tubes] were shown to have significantly lower interfacial formation energy than larger ones. This was in agreement with our experimental results.

For better understanding of the enrichment process with TPCVD, especially supporting the plate model, we grew SWNTs with perturbation cycles varying from 0 to 90 with steps of 30 cycles, and the results were shown in Fig. 3 (A to D). From the SEM images, we noticed that after many cycles of the temperature perturbation, the average length, and the density of the SWNTs decreased. This might be partially attributed to the poisoning of the catalysts and partially due to the low
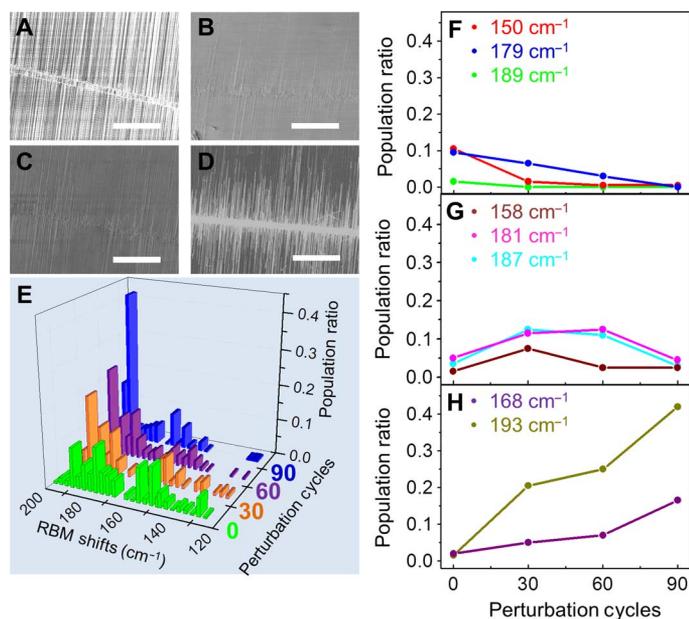
Fig. 3. Dynamic analysis of TPCVD and the classification of SWNT structures. (**A** to **D**) SEM image of SWNT arrays with different times of temperature perturbation, representing 0, 30, 60, and 90 cycles, respectively. The decreasing length of SWNT might be caused by the catalyst inactivation. Scale bars, 50 μm. (**E**) Raman analysis of different RBM distributions. Bars in green, orange, purple, and blue refer to samples after 0, 30, 60, and 90 temperature perturbation cycles, respectively. The significant enrichment process was investigated. SWNT arrays after transfer onto a SiO$_x$/Si substrate. The excitation laser frequency was 514 nm. More than 500 RBM signals were collected for each sample. (**F** to **H**) Three types of SWNT structures, representing types A, B, and C, separately. Type A structures were those that decrease with the number of perturbation cycles. Type B showed an increasing trend when perturbation cycles increased at first and then a decrease when perturbation cycles increased further. Type C increased continuously.

growth rates of zigzag or near-zigzag SWNTs. Following the well recognized vapor-liquid-solid mechanism, one can easily understand that the rapid temperature variation would lead to a rapid change of carbon solubility in catalysts. In each temperature perturbation cycle, the fast precipitation of carbon from the catalyst during the cooling process may lead to the accumulation of amorphous carbon on the catalyst surface and the poisoning of catalyst. Raman mapping with a 514-nm laser was also used to detect the dynamic process. Figure 3E shows the statistics of the RBM peaks. From these, we could easily observe the enrichment of some specific RBM shifts, such as peaks near 193 and 168 cm^{-1}. Some SWNTs with specific structures were selected to analyze the physics that governed the change. Three different types of peak variations were classified, as shown in Fig. 3 (F and G). The relative population of type A, corresponding to large chiral SWNTs such as (13,11) and (11,9), was observed to decrease with an increase in perturbation cycles. Type C, those for small chiral angle SWNTs such as (15,2) and (17,3), kept increasing with perturbation cycles. The third class, type B, normally corresponding to medium chiral angle SWNTs such as (13,6), showed an initial increase in population and then a decrease as the number of perturbation cycles was varied from 0 to 90. Besides the

reported 30, 60, and 90 cycles, we also tried more cycles. However, the results show that more temperature perturbation cycles than 90 (such as 120) cannot improve the results further. A potential reason for that may be due to the very slow growth rate of zigzag SWNTs or the deactivation of the catalysts, discussed above.

Besides type C, types A and B showed that our system was more complicated than a two-component equilibrium system. Features of these three types of SWNT variations are similar to the concentration variation in the so-called consecutive reaction, in which type A were compared to the reactants, type B were compared to the intermediate products, and type C were compared to the final products. Thus, we made a surface mapping of SWNT horizontal arrays with an excitation laser wavelength of 532 nm for a deeper analysis of chirality changes. Typical intramolecular junctions were found in individual tubes, as shown in Fig. 4A. The catalyst stripe was below the inset figure, out of the picture. For the base growth mechanism, we could clearly differentiate the initial and final structure of the intramolecular junction. The three types classified above were used to analyze the rules governing the chirality change during the TPCVD process, as shown in Fig. 4B. We found that the transformations from A to B and from B to C were more probable than other routes, such as the change from type A to C directly. The helix angles of these three types of SWNTs showed a downward trend from A to C. This phenomenon shows that a gradual change, rather than an abrupt one between small and large helix angle, was preferred.

For a deeper understanding of the different chirality transition routes, we made theoretical calculations, as shown in Fig. 4C. We found that the intratube transformations with small (<5°) and large (>25°) angle differences had lower formation energy penalties, presenting a relatively lower activation gap and a higher probability for these routes. However, the formation energy of medium helix angle differences was much higher.

DISCUSSION

On the basis of the above, we proposed a mechanism for the TPCVD process, as illustrated in Fig. 4D. The intratube formation energy barrier between armchair and zigzag structures is relatively small, allowing easy transfer between these structures. However, armchair tubes are not present in high proportions in the initial structure, and the final zigzag structure is inhibited by kinetic disadvantages, making it difficult for these junctions to be observed. For other SWNTs with a smaller helix angle (<25°), one-step transfer would have a big energy gap, thus limiting them kinetically. Therefore, the trend should be for tubes to follow a step-by-step transfer model. At each step, the helix angle should only make a small change (<5°). According to the simulation, junctions with small helix angle change have lower formation energy. This endows our CVD process with both a dynamic picture of consecutive reaction and a step-by-step equilibrium processing like plates in distillation column, which is therefore called "tandem plate" to highlight the similarity in concept.

In summary, we designed a TPCVD method to enrich SWNTs with small helix angles. The contribution of SWNT-catalyst interfacial formation energy in the SWNT chirality control was proven both experimentally and theoretically. The role of intratube junction formation energy in the tube chirality variation was also investigated and found to support the experimentally observed step-by-step chirality
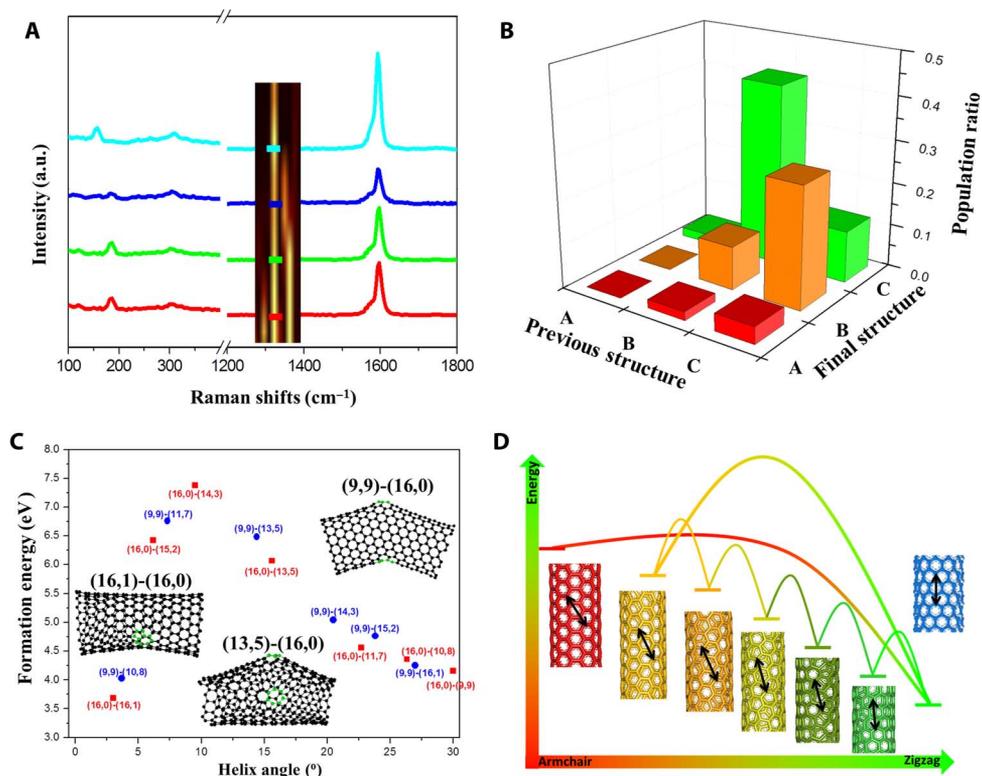
Fig. 4. Statistics and theoretical analysis of intratube junction. (**A**) G-band Raman mapping of an individual SWNT (inset) and the RBM peaks along the tube. An intramolecular junction was evident. The lowest position (shown in red) was closer to the catalyst stripe and was grown later in the TPCVD method. a.u., arbitrary unit. (**B**) Statistics of intratube junctions. In total, 50 junctions were analyzed, and the routes of A to B and B to C were found most frequently. (**C**) Formation energy of intratube junctions with different angle differences. The junctions with small (<5°) and large (>25°) angle differences had lower formation energy. Insets showed geometric structures of intratube junctions with different angle differences. (**D**) Schematic illustration of the TPCVD process.

change. Last but not least, this method provided a broad platform for achieving chirality-selective SWNT growth by theoretical catalyst design. The enrichment of any SWNTs with low SWNT-catalyst interfacial formation energy, including those with specific electronic properties, certain helix angle ranges, or even single chirality, might be achieved with our TPCVD process by careful catalyst design.

MATERIALS AND METHODS

Growth of normal SWNT arrays

ST-cut quartz substrates (single-side polished; miscut angle, <0.5°; surface roughness, <5 Å) were purchased from Hefei Kejing Materials Technology Co. After cleaning, the quartz substrates were annealed at 900°C in air for 8 hours followed by cooling to 300°C over 10 hours to enhance crystallization. A total of 0.05 mM $Fe(OH)_3$/ethanol collosol, which was used as a catalyst precursor, was dispersed onto the substrates. The catalyst stripes were patterned onto the substrate by a needle after dipping into the catalyst precursor solution. SWNT growth was performed in a furnace with a 1-inch tube. The quartz substrates with well dispersed iron species were put into the tube and heated in air from room temperature to 850°C in 20 min. Then, the system was purged with 300-sccm (standard cubic centimeters per minute) argon

for 5 min. After that, 300-sccm H_2 was purged for 5 min, and then argon (30 sccm; through an ethanol bubbler) was introduced for the growth of SWNT arrays at 850°C for 15 min. Finally, the sample was cooled to below 200°C naturally under the protection of Ar.

Growth of TPCVD SWNT arrays

At first, the above process up to the 300-sccm H_2 treatment was followed. After H_2 treatment, argon (30 sccm; through an ethanol bubbler) was introduced, and a 5-min pregrowth process was implemented at 850°C. The next step involved temperature modulation, achieved by moving the furnace to control the sample position moving repeatedly from $\Delta L = 0$ cm to $\Delta L = 7$ cm, which changes the temperature at sample position from 880° to 820°C. The moving process was done in 1 s and followed by a 5-s pause for temperature stabilization. At the end of the temperature perturbation, a 5-min postgrowth process at 850°C was also implemented. The cooling down process was similar to normal growth.

Basic characterization of as-grown SWNT arrays

The as-grown SWNTs were inspected with SEM (Hitachi S-4800 field emission), atomic force microscopy (Veeco NanoScope IIIA), and TEM (Tecnai F30, Philips-FEI) to characterize their morphology and structure.

Raman characterization of as-grown SWNT arrays

Line mapping was inspected with Raman (HR800). Three excitation energies—514, 633, and 785 nm—were used to cover more than 50% of chiralities. The scanning line was 5 μm away from the catalyst stripes on each sample. Because we had a postgrowth process at 850°C, SWNTs with the final structure after temperature perturbation could grow for a certain length, which was believed to be no shorter than 5 μm (typically more than 100 μm for 15 min in our CVD system). Area mapping was inspected with a 532-nm laser using another Raman (WITec, alpha300).

Details of DFT calculation

The Vienna Ab Initio Simulation Package was used for DFT calculations (35, 36). By using the Perdew-Burke-Ernzerhof functional, the generalized gradient approximation was adopted for the exchange correlation, with spin polarization taken into account (37). The plane wave cutoff energy was set at 400 eV, and the projector-augmented wave was used as the pseudopotential (38). The convergence criterion for energy and force was set at 10^{-4} eV and 0.01 eV/Å, respectively.

Definition of interfacial formation energy

The interfacial formation energy (IFE; E_f) of an SWNT on a Fe_{55} particle was

$$E_f = E_{FE} - E_b \tag{1}$$

in which E_{FE} and E_b were the formation energy of the free SWNT end and the SWNT-metal binding energy, respectively, and E_b was

$$E_b = E_{NT} + E_{Fe} - E_{NT@Fe} \tag{2}$$

in which $E_{NT@Fe}$ was the energy of SWNT attached to Fe_{55}, and E_{NT} and E_{Fe} were energies of the isolated SWNT and Fe_{55}, respectively. E_{FE} in Eq. 2 was

$$E_{FE} = 0.5 * (2 * E_{NT2} - E_{NT1}) \tag{3}$$

in which E_{NT1} was the energy of a longer SWNT, and E_{NT2} was the energy of a shorter SWNT obtained by cutting the longer SWNT into two equal segments. The factor 0.5 referred to the fact that two open ends were formed when an SWNT was cut into two shorter SWNTs.

Calculation of the formation energy of an intratube junction

As shown in Fig. 4C, we constructed a series of intratube junctions (containing only one pentagon and one heptagon) by connecting two SWNT stems with different chiralities but similar diameters (see the chirality map of the selected tubes). The chiral angle difference between the two sides could cover the range of 0° to 30°. All of the energies of the optimized structures were calculated by the adaptive intermolecular reactive empirical bond order potential (39). The formation energy of the junction was defined as

$$E_F = E_{JUN} - e_1 * n_1 - e_2 * n_2 - E_{EF1} - E_{EF2} \tag{4}$$

where E_{JUN} was the optimized energy of the constructed junction, e_1 and e_2 were the two energies of each carbon atom located in the inner section of the two connected tubes, and n_1 and n_2 were the numbers of the carbon atoms belonging to the two sides of the tube. E_{EF1} and E_{EF2}

were the edge energies of the open ends of the two connected tubes, the definition of which was similar to Eq. 3. Note that there was an attribution issue with the carbon atoms near the intersection of pentagon and heptagon. Considering the very small energy difference ($|e_1 - e_2|$ ~0.001 eV/carbon) of the inner tubes with different structures, for simplicity, we usually divided the atoms near the intersection of pentagon and heptagon equally into two sides. The uncertainty of the formation energy of the junction caused by this artificial division of the carbon atoms does not exceed ~0.01 eV, which does not influence the final conclusions.

REFERENCES AND NOTES

1. Y. Chen, J. Zhang, Chemical vapor deposition growth of single-walled carbon nanotubes with controlled structures for nanodevice applications. Acc. Chem. Res. **47**, 2273–2281 (2014).
2. S. M. Bachilo, L. Balzano, J. E. Herrera, F. Pompeo, D. E. Resasco, R. B. Weisman, Narrow (n,m)-distribution of single-walled carbon nanotubes grown using a solid supported catalyst. J. Am. Chem. Soc. **125**, 11186–11187 (2003).
3. L. An, J. M. Owens, L. E. McNeil, J. Liu, Synthesis of nearly uniform single-walled carbon nanotubes using identical metal-containing molecular nanoclusters as catalysts. J. Am. Chem. Soc. **124**, 13688–13689 (2002).
4. G. Lolli, L. Zhang, L. Balzano, N. Sakulchaicharoen, Y. Tan, D. E. Resasco, Tailoring (n,m) structure of single-walled carbon nanotubes by modifying reaction conditions and the nature of the support of CoMo catalysts. J. Phys. Chem. B **110**, 2108–2115 (2006).
5. X. Li, X. Tu, S. Zaric, K. Welsher, W. S. Seo, W. Zhao, H. Dai, Selective synthesis combined with chemical separation of single-walled carbon nanotubes for chirality selection. J. Am. Chem. Soc. **129**, 15770–15771 (2007).
6. W.-H. Chiang, R. M. Sankaran, Linking catalyst composition to chirality distributions of as-grown single-walled carbon nanotubes by tuning Ni_xFe_{1-x} nanoparticles. Nat. Mater. **8**, 882–886 (2009).
7. H. Wang, L. Wei, F. Ren, Q. Wang, L. D. Pfefferle, G. L. Haller, Y. Chen, Chiral-selective $CoSO_4/SiO_2$ catalyst for (9,8) single-walled carbon nanotube growth. ACS Nano **7**, 614–626 (2013).
8. F. Yang, X. Wang, D. Zhang, J. Yang, D. Luo, Z. Xu, J. Wei, J.-Q. Wang, Z. Xu, F. Peng, X. Li, R. Li, Y. Li, M. Li, X. Bai, F. Ding, Y. Li, Chirality-specific growth of single-walled carbon nanotubes on solid alloy catalysts. Nature **510**, 522–524 (2014).
9. F. Yang, X. Wang, D. Zhang, K. Qi, J. Yang, Z. Xu, M. Li, X. Zhao, X. Bai, Y. Li, Growing zigzag (16,0) carbon nanotubes with structure-defined catalysts. J. Am. Chem. Soc. **137**, 8688–8691 (2015).
10. E. S. Penev, V. I. Artyukhov, B. I. Yakobson, Extensive energy landscape sampling of nanotube end-caps reveals no chiral-angle bias for their nucleation. ACS Nano **8**, 1899–1906 (2014).
11. Y. Yao, C. Feng, J. Zhang, Z. Liu, "Cloning" of single-walled carbon nanotubes via open-end growth mechanism. Nano Lett. **9**, 1673–1677 (2009).
12. J. Liu, C. Wang, X. Tu, B. Liu, L. Chen, M. Zheng, C. Zhou, Chirality-controlled synthesis of single-wall carbon nanotubes using vapour-phase epitaxy. Nat. Commun. **3**, 1199 (2012).
13. F. Ding, A. R. Harutyunyan, B. I. Yakobson, Dislocation theory of chirality-controlled nanotube growth. Proc. Natl. Acad. Sci. U.S.A. **106**, 2506–2509 (2009).
14. X. Yu, J. Zhang, W. Choi, J.-Y. Choi, J. M. Kim, L. Gan, Z. Liu, Cap formation engineering: From opened C_{60} to single-walled carbon nanotubes. Nano Lett. **10**, 3343–3349 (2010).

15. J. R. Sanchez-Valencia, T. Dienel, O. Gröning, I. Shorubalko, A. Mueller, M. Jansen, K. Amsharov, P. Ruffieux, R. Fasel, Controlled synthesis of single-chirality carbon nanotubes. *Nature* **512**, 61–64 (2014).

16. V. I. Artyukhov, E. S. Penev, B. I. Yakobson, Why nanotubes grow chiral. *Nat. Commun.* **5**, 4892 (2014).

17. L. Kang, Y. Hu, L. Liu, J. Wu, S. Zhang, Q. Zhao, F. Ding, Q. Li, J. Zhang, Growth of close-packed semiconducting single-walled carbon nanotube arrays using oxygen-deficient TiO$_2$ nanoparticles as catalysts. *Nano Lett.* **15**, 403–409 (2015).

18. L. Li, S. Reich, J. Robertson, Modelling the nucleation and chirality selection of carbon nanotubes. *J. Nanosci. Nanotechnol.* **6**, 1290–1297 (2006).

19. S. Reich, L. Li, J. Robertson, Control the chirality of carbon nanotubes by epitaxial growth. *Chem. Phys. Lett.* **421**, 469–472 (2006).

20. S. Reich, L. Li, J. Robertson, Structure and formation energy of carbon nanotube caps. *Phys. Rev. B* **72**, 165423 (2005).

21. O. V. Yazyev, A. Pasquarello, Effect of metal elements in catalytic growth of carbon nanotubes. *Phys. Rev. Lett.* **100**, 156102 (2008).

22. M. He, H. Jiang, B. Liu, P. V. Fedotov, A. I. Chernov, E. D. Obraztsova, F. Cavalca, J. B. Wagner, T. W. Hansen, I. V. Anoshkin, E. A. Obraztsova, A. V. Belkin, E. Sairanen, A. G. Nasibulin, J. Lehtonen, E. I. Kauppinen, Chiral-selective growth of single-walled carbon nanotubes on lattice-mismatched epitaxial cobalt nanoparticles. *Sci. Rep.* **3**, 1460 (2013).

23. S. M. Bachilo, M. S. Strano, C. Kittrell, R. H. Hauge, R. E. Smalley, R. B. Weisman, Structure-assigned optical spectra of single-walled carbon nanotubes. *Science* **298**, 2361–2366 (2002).

24. A. Jorio, R. Saito, J. H. Hafner, C. M. Lieber, M. Hunter, T. McClure, G. Dresselhaus, M. S. Dresselhaus, Structural (n, m) determination of isolated single-wall carbon nanotubes by resonant Raman scattering. *Phys. Rev. Lett.* **86**, 1118 (2001).

25. M. Fouquet, B. C. Bayer, S. Esconjauregui, R. Blume, J. H. Warner, S. Hofmann, R. Schlögl, C. Thomsen, J. Robertson, Highly chiral-selective growth of single-walled carbon nanotubes with a simple monometallic Co catalyst. *Phys. Rev. B* **85**, 235411 (2012).

26. H. Wang, B. Wang, X.-Y. Quek, L. Wei, J. Zhao, L.-J. Li, M. B. Chan-Park, Y. Yang, Y. Chen, Selective synthesis of (9, 8) single walled carbon nanotubes on cobalt incorporated TUD-1 catalysts. *J. Am. Chem. Soc.* **132**, 16747–16749 (2010).

27. Q. Wen, W. Qian, J. Nie, A. Cao, G. Ning, Y. Wang, L. Hu, Q. Zhang, J. Huang, F. Wei, 100 mm long, semiconducting triple-walled carbon nanotubes. *Adv. Mater.* **22**, 1867–1871 (2010).

28. Q. Yuan, Z. Xu, B. I. Yakobson, F. Ding, Efficient defect healing in catalytic carbon nanotube growth. *Phys. Rev. Lett.* **108**, 245505 (2012).

29. Y. Yao, Q. Li, J. Zhang, R. Liu, L. Jiao, Y. T. Zhu, Z. Liu, Temperature-mediated growth of single-walled carbon-nanotube intramolecular junctions. *Nat. Mater.* **6**, 283–286 (2007).

30. Y. Yao, X. Dai, R. Liu, J. Zhang, Z. Liu, Tuning the diameter of single-walled carbon nanotubes by temperature-mediated chemical vapor deposition. *J. Phys. Chem. C* **113**, 13051–13059 (2009).

31. C. Feng, Y. Yao, J. Zhang, Z. Liu, Nanobarrier-terminated growth of single-walled carbon nanotubes on quartz surfaces. *Nano Res.* **2**, 768–773 (2009).

32. Q. Yuan, F. Ding, How a zigzag carbon nanotube grows. *Angew. Chem. Int. Ed.* **54**, 5924–5928 (2015).

33. Q. Zhao, J. Zhang, Characterizing the chiral index of a single-walled carbon nanotube. *Small* **10**, 4586–5605 (2014).

34. Y. Hu, L. Kang, Q. Zhao, H. Zhong, S. Zhang, L. Yang, Z. Wang, J. Lin, Q. Li, Z. Zhang, L. Peng, Z. Liu, J. Zhang, Growth of high-density horizontally aligned SWNT arrays using Trojan catalysts. *Nat. Commun.* **6**, 6099 (2015).

35. P. E. Blöchl, Projector augmented-wave method. *Phys. Rev. B* **50**, 17953 (1994).

36. G. Kresse, J. Furthmuller, Efficient iterative schemes for *ab initio* total-energy calculations using a plane-wave basis set. *Phys. Rev. B* **54**, 11169 (1996).

37. J. P. Perdew, K. Burke, M. Ernzerhof, Generalized gradient approximation made simple. *Phys. Rev. Lett.* **77**, 3865 (1996).

38. G. Kresse, D. Joubert, From ultrasoft pseudopotentials to the projector augmented-wave method. *Phys. Rev. B* **59**, 1758 (1999).

39. S. J. Stuart, A. B. Tutein, J. A. Harrison, A reactive potential for hydrocarbons with intermolecular interactions. *J. Chem. Phys.* **112**, 6472 (2000).

Science Advances

Chemical vapor deposition synthesis of near-zigzag single-walled carbon nanotubes with stable tube-catalyst interface

Qiuchen Zhao, Ziwei Xu, Yue Hu, Feng Ding and Jin Zhang

ARTICLE TOOLS	http://advances.sciencemag.org/content/2/5/e1501729
SUPPLEMENTARY MATERIALS	http://advances.sciencemag.org/content/suppl/2016/05/10/2.5.e1501729.DC1
REFERENCES	This article cites 39 articles, 2 of which you can access for free http://advances.sciencemag.org/content/2/5/e1501729#BIBL
PERMISSIONS	http://www.sciencemag.org/help/reprints-and-permissions

Use of this article is subject to the Terms of Service